PCCP

Extending Graphene Oxide Aromaticity for Superior Capacitive Energy Storage and Photoluminescence Applications

Journal:	*Physical Chemistry Chemical Physics*
Manuscript ID	CP-ART-11-2015-007254.R1
Article Type:	Paper
Date Submitted by the Author:	10-Feb-2016
Complete List of Authors:	Eng, Alex Yong Sheng; Nanyang Technological University, Chua, Chun Kiang; Nanyang Technological University, Chemistry and Biological Chemistry Pumera, Martin; Nanyang Technological University, Chemistry and Biological Chemistry

Facile Labelling of Graphene Oxide for Superior Capacitive Energy Storage and Fluorescence Applications

*Alex Yong Sheng Eng, Chun Kiang Chua, Martin Pumera**

Division of Chemistry & Biological Chemistry, School of Physical and Mathematical Sciences, Nanyang Technological University, Singapore 637371, Singapore.

KEYWORDS: graphene, graphene oxide, covalent functionalization, electrical conductivity, supercapacitor, pseudo-capacitance, photoluminescence, fluorescence.

Abstract

The majority of supercapacitor research on graphene materials today has been based upon developing electrochemical double-layer capacitors (EDLCs) using reduced graphenes. In contrast, graphene oxide (GO) is often neglected as a supercapacitor candidate due to its low electrical conductivity and surface area. Nonetheless, we present herein a fast (1 h) labelling of GO with *o*-phenylenediamine (PD) to produce PD-GO, exploiting inherent oxygen groups in creating new functionalities that exhibit capacitive enhancement from pseudo-capacitance. A

high specific capacitance of 191 F g^{-1} was obtained (at 0.2 A g^{-1}), comparable to recent binder-free graphene supercapacitors. The large surface-normalized capacitance of up to 628 μF cm^{-2} is also many times greater than the intrinsic capacitance of single-layer graphene (21 μF cm^{-2}) as a result of additional pseudo-capacitance. High capacity retention of ~85% with each 10-fold increase in current density further indicates excellent rate performance. Hence, this approach in enhancing GO pseudo-capacitance may be similarly feasible as graphene EDLCs. Additionally, PD-GO was also found to exhibit a bright green fluorescence with a 540 nm maximum. Strongest fluorescence intensities arose from the smallest PD-GO fragments, and we attribute the origin to localised sp^2 domains and newly formed phenazine edge groups. The dual enhancement of dissimilar properties such as capacitance and fluorescence emphasizes the continued significance of covalent functionalisation towards tuning of properties in graphene-type materials.

1. Introduction

It is well-accepted that graphene as the two-dimensional sp^2 carbon allotrope possesses numerous fundamental properties sought after for electronics, energy storage[1-6] and optical devices.[7,8,9] In its pristine state, graphene possesses high electrical conductivity due to extended sp^2 conjugation, where its aromatic character may be described as localised with each carbon hexagonal ring bearing two delocalized π-electrons.[10,11] In practice however, properties vary with preparation technique and these advantageous qualities are not always realized. Graphene-based supercapacitors are one such interesting case in point. With an intrinsic capacitance of *ca*. 21 μF cm^{-2},[12] a theoretical specific capacitance of 550 F g^{-1} is purported to be achievable for single-layer graphene due to its large surface area.[13] Many groups have employed a variety of means to

achieve such a large capacitance, such as through enhancing the *electrochemical double layer capacitor* (EDLC) character of graphite/reduced graphenes using treatments to increase the active surface area (*eg.* hydrogels,[14] sheet crumpling[15,16] or ball milling[17,18]). However, preparation methods inadvertently introduce defects and oxygen groups, rendering any comparison to pristine graphene erroneous. Increasingly, computational[19,20,21] and experimental[22,23,24] evidence show that defects and functionalities are instead the main contributors to the measured capacitance, which we explore in this paper. This leads us to the second *pseudo-capacitive* route towards developing graphene-based supercapacitors, which to date usually involves mixing/functionalization of GO with a secondary electroactive/conductive material such as polyaniline (PANI),[25-27] or carbon nanotubes.[28,29] One important objective within both directions is the common need to achieve electrical conductivity, either intrinsically maintained from graphene or from an additive (*eg*. carbon black)[28] to the insulator GO. We note however, a lack of attempts to enhance the inherent pseudo-capacitance of GO, especially while addressing conductivity issues.

Another distinction between GO and graphene is that GO exhibits fluorescence or photoluminescence (PL) under specific conditions, but is entirely absent from pure graphene which lacks a bandgap.[8,9] Although exact mechanisms have yet to be confirmed definitively,[9,30] it is generally agreed to be due to a bandgap opening from functional groups and their confinement of isolated sp^2 hybridised domains.[31-34] It must be further emphasized that the observed PL intensities and wavelengths from GO are heavily dependent on factors such as the oxidation extent and size of localized sp^2 regions. GO can also act as a fluorescence quencher if a significantly high concentration of sp^2 domains exist leading to greater non-radiative

recombinations.[9,34,35] Hence, attempts at precise control of factors influencing GO fluorescence and quenching is made very challenging due to the vast heterogeneity of GO materials, and functionalization with reactive moieties may therefore be a more promising route for better control of photoluminescence.[35,36]

In light of the plentiful functionalities available in GO, we exploit these moieties to enhance the electrical conductivity, capacitive charge storage, and fluorescence of GO simultaneously together for the first time. The rational design of such a multifunctional GO material is performed by a facile one-step labelling reaction with 1,2-phenylenediamine (PD). PD labelling of GO to PD-GO creates new aromatic phenazine adducts[37,38] at the sheet edges (Scheme 1) upon reaction with the *o*-quinone moieties present in GO.[39,40] This firstly increases the overall electrical conductivity of the material. Furthermore, the specific capacitance increases by more than two orders of magnitude, from pseudo-capacitance of the phenazine adducts.[37,38] Fluorescence is also observed from the labelled GO, as a result of changes brought about by the labelling of edge sites and also other reactive groups[41,42] on the basal plane such as the epoxyls in large abundance.

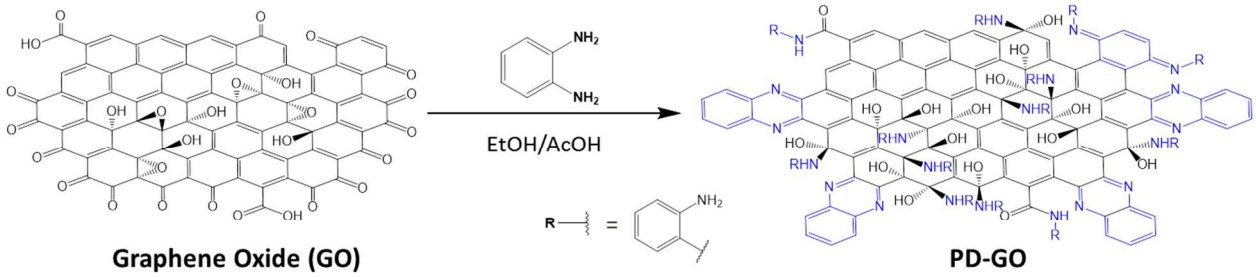

Scheme 1. Synthetic labelling of various graphene oxide inherent functional groups with 1,2-phenylenediamine (PD), both at the basal plane and edges.

2. Results and Discussion

We first investigate the process of graphene oxide labelling with PD in terms of its chemical nature using X-ray photoelectron spectroscopy (XPS) and energy-dispersive X-ray spectroscopy (EDS), while structural morphology is probed using a combination of Raman spectroscopy and scanning transmission electron microscopy (STEM). As seen in Figure 1a, wide-scan XPS shows only carbon-1s and oxygen-1s peaks present in the parent GO with a carbon-to-oxygen (C/O) ratio of 2.65 that is typical of most GOs.[43,44] The C/O ratio increases to 5.61 after PD labelling, and now includes a new nitrogen-1s peak at 4.93 at.%. The concomitant decrease in oxygen content agrees well with the reaction scheme involving a hydrolysis reaction between PD and *o*-quinonyls, and also nucleophilic acyl substitution on carboxyl sites with the loss of water. It is also important to highlight that the labelling procedure does not constitute a reduction of GO as the C/O ratio of PD-GO remains low, in contrast to a much higher 10.3 for the case of reduced-GO.[44] Examining changes to the carbon-1s XPS region in Figure 1b, we note a significant decrease in the C-O and C=O contributions at approximately 286.3 eV and 287.4 eV corresponding to the PD reaction with epoxide and carbonyl groups, respectively.[43,45] High resolution scans of the nitrogen-1s region demonstrates two characteristic peaks at *ca*. 398.5 eV from pyrazine nitrogen affirming the labelling of *o*-quinones, and at 400 eV from arylamine produced upon epoxyl and carboxylic functionalization.[46,47] Additionally, we confirm that non-specific adsorption does not occur from further control experiments with nitrobenzene.[48] Hence, these data provide definitive proof for covalent labelling between PD and the individual functional groups in GO. From STEM imaging (Figure 1c), it is observed that the mild labelling procedure did not have considerable effect on the structure of large GO sheets. Subsequently, EDS mapping analysis corroborates with the XPS results illustrating only carbon and oxygen in

the parent GO, and also the appearance of nitrogen throughout the basal plane of PD-GO indicating a successful labelling reaction.

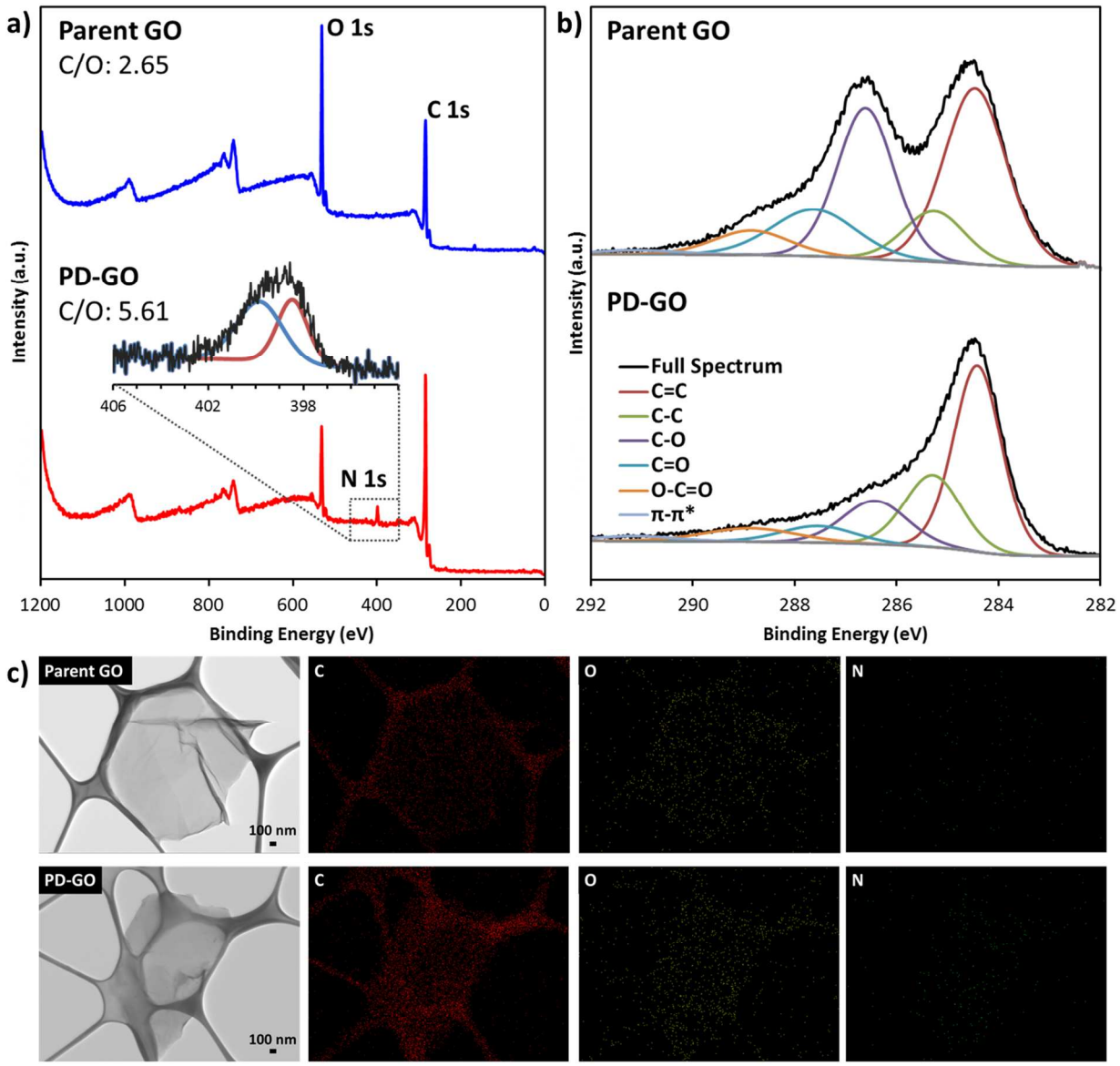

Figure 1. Structural and chemical analysis of graphene oxide before and after chemical labelling with PD. **a)** Wide-scan X-ray photoelectron spectra of parent GO and PD-GO (Inset: high resolution scan of nitrogen 1s region); **b)** high resolution carbon 1s spectra of parent GO and PD-

GO; **c)** scanning transmission electron micrographs with elemental mapping from energy-dispersive X-ray spectroscopy of parent GO and PD-GO.

Consequently, a comparison of electrical conductivities between the parent and labelled PD-GO is performed. From the current-voltage curves of the materials performed on interdigitated gold electrodes (Figure 2a), both materials exhibited near-ideal Ohmic behavior with curves close to linearity. The *I-V* slope of GO is expectedly low with an average conductance of just 8.24×10^{-4} mS. PD-GO in contrast demonstrated an improved conductance by almost three orders of magnitude to 0.185 mS. This change is corroborated with optical darkening of PD-GO as seen in Figure 2b. Also, the improved conductance of PD-GO is still lower than that of chemically-reduced GO (~75 mS) indicating that surface functionalities remain intact.[49]

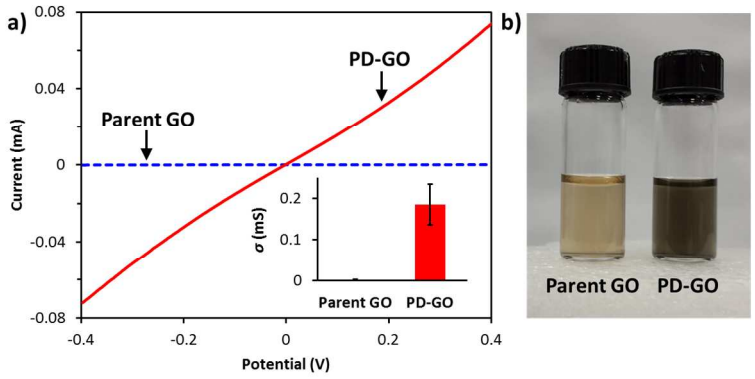

Figure 2. a) Current-voltage curves of the parent GO and PD-GO as measured on interdigitated gold electrode. Inset: Comparison of electrical conductance. Error bars represent the standard deviation based on triplicate measurements. **b)** Dispersions of parent GO and PD-GO in *N*,*N*-dimethylformamide at 0.1 mg mL^{-1}, with optical darkening observed after PD-labelling.

With affirmation on the conductivity of PD-GO, we next investigate its capacitive storage ability by first employing the cyclic voltammetry technique in aqueous 6 M KOH electrolyte. Figure 3a illustrates the difference in capacitive voltammograms obtained for GO before and after labelling at 0.1 V s^{-1}. The parent GO only exhibits a very small capacitance of approximately 1-2 F g^{-1} similar to a previous report (0.9 F g^{-1}),[50] and remains relatively constant at varying scan rates (Figure 3b). In terms of wave shape, both the parent GO and PD-GO demonstrate typical wide rectangular-shaped voltammograms characteristic of EDLCs but with deviations which indicate additional pseudo-capacitive contributions[51,52] from their inherent oxygen functionalities. Closer inspection of PD-GO voltammograms also reveals a set of Faradaic redox peaks at −0.4 V and −0.55 V *vs*. Ag/AgCl, and most likely arise from labelled phenazine adducts at the sheet edges as they correspond to previously reported potentials.[37,38] No obvious effect was seen when the charging rate was varied as with the case of the GO parent (Figure 3c). Galvanostatic cycling was next employed to study the labelled GO, as seen in Figure 3d at increasing current densities. PD-GO displayed expected EDLC-type triangular-shaped charge/discharge cycles, with tapering of the charging potential occurring only at the lowest 0.2 A g^{-1} current density used likely as more pores are accessed by the electrolyte. At this current density, PD-GO exhibits a much superior capacitor ability to the parent GO with a high specific capacitance of 191 F g^{-1}. This is two orders of magnitude greater than parent GO measured at 1.37 F g^{-1}, and is also considerably larger than other graphene-type materials[50] such as graphite microparticles (0.88 F g^{-1}), chemically-reduced graphene (1.14 F g^{-1}), and even thermally-reduced graphene (26.1 F g^{-1}) with its characteristically large specific surface area. The capacitance of PD-GO was also observed to be larger than the 169 F g^{-1} value recently reported for a high surface area binder-free graphene supercapacitor in the same electrolyte.[14] Hence, the

idea of enhancing GO pseudo-capacitance may very well be a viable approach for supercapacitor design in addition to the more common approach of increasing the surface area of graphene, on condition that the electrical conductivity of GO is also improved.

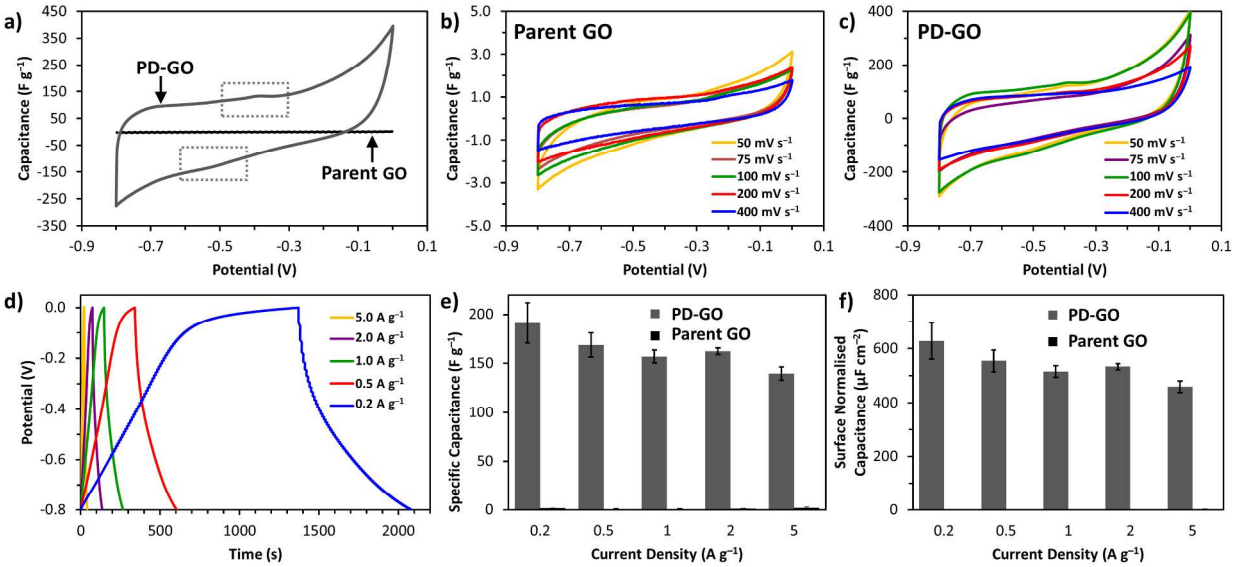

Figure 3. Supercapacitor performances of parent GO and PD-GO in 6 M KOH. **a)** Cyclic voltammograms of parent GO and PD-GO at 100 mV s^{-1} (boxed regions indicate pseudocapacitance of benzophenazine adduct after PD labelling); **b)** voltammograms of parent GO at varying scan rates; **c)** voltammograms of PD-GO at varying scan rates; **d)** galvanostatic charge-discharge curves of parent GO and PD-GO at varying current densities; **e)** specific capacitance and **f)** surface-normalized capacitance of parent GO and PD-GO at varying current densities.

We then further evaluated the *rate performance* of the capacitor for a consistent comparison with other previously studied materials.[53] The specific capacitance of PD-GO follows the expected decrease as current density is increased (Figure 3e). However, the capacitance is maintained at a relatively high value of 162 F g^{-1} when measured with a 10-fold higher current

density at 2.0 A g^{-1}. This translates to an 85% capacity retention to the 191 F g^{-1} at 0.2 A g^{-1}. The retention is similarly high at 83% comparing between the measured capacitances at 0.5 A g^{-1} and 5.0 A g^{-1}, thus signifying the excellent rate capability of PD-GO.

Considering that surface areas can have a major influence on the gravimetric capacitance,[23] normalization of capacitances was also done to the Brunauer-Emmett-Teller (BET) surface areas. The BET surface area of the parent GO was determined to be 96.9 m^2 g^{-1}, and interestingly decreased to 30.4 m^2 g^{-1} for PD-GO (Supporting Information Figure S1). Nevertheless, the smaller surface area is a likely outcome of sheet re-stacking from stronger overall van der Waals forces resulting from PD-labelling. As such, the surface area-normalized capacitance of PD-GO was found to be a large 628 μF cm^{-2} compared to just 1.42 μF cm^{-2} for the parent GO. This is juxtaposed to a low theoretical intrinsic capacitance for single-layer graphene[12] and empirically-determined for reduced graphene,[14] both in agreement at approximately 21 μF cm^{-2}. We also considered the possibility that differences in pore-size may have resulted in the increased capacitance of PD-GO,[4,54,55] and further utilize the non-local density functional theory (NLDFT) method for their pore-size distributions (Figure S1c-d). Both the parent and PD-GO were found to consist primarily of narrow meso-pores with a maximum pore width close to 3 nm and increasing to 10 nm. However, only the parent GO contained micro-pores (< 2 nm) and these are absent in PD-GO, likely due to PD functionalization at oxygen groups which typically decorate the boundary of vacancies and edge-like defects. Thus in spite of the pore size effect of ion desolvation in carbon micro-pores known to result in larger specific capacitance,[54,55] the capacitance of parent GO still remained lower than PD-GO. In summary, parent GO capacitance remained low notwithstanding a higher surface area, micro-pore structure and its numerous

inherent oxygen functionalities. Hence, the superior PD-GO capacitance must therefore arise from a combination of pseudo-capacitance from newly labelled moieties (*eg*. phenazine) and the restoration of electrical conductivity.

GO is also unique in its ability to exhibit fluorescence over a range of wavelengths under different environments; factors influencing these properties include size of sp^2 domains, size confinement effects (*eg*. quantum dots), defect sites, or functionalities.[8,9,32-34] Figure 4a shows the excitation-emission map of the parent GO which displays no fluorescence except for a broad emission band from 420 nm to 540 nm that is also observed in PD-GO (Figure 4b). Control experiments using pure DMF and PD in solution confirm the origin to be from GO itself (Figure S2). More prominently, no emission near 500-600 nm was seen as reported by some reports on GO.[30,31] In the labelled PD-GO however, fluorescence was observed when excited at several wavelengths but only emitted over a single broad band from 460 nm to 640 nm (Figure 4b). A greenish glow was observable when the PD-GO dispersion was irradiated with UV light at 365 nm (Figure 4c). The lack of such fluorescence in the control GO (Figure S3) prepared under similar conditions confirm PD-labelling to be responsible. When excited at 290 nm and 430 nm in Figure 4d-e, PD-GO displays a broad peak with a same maximum at 540 nm for both excitation wavelengths.

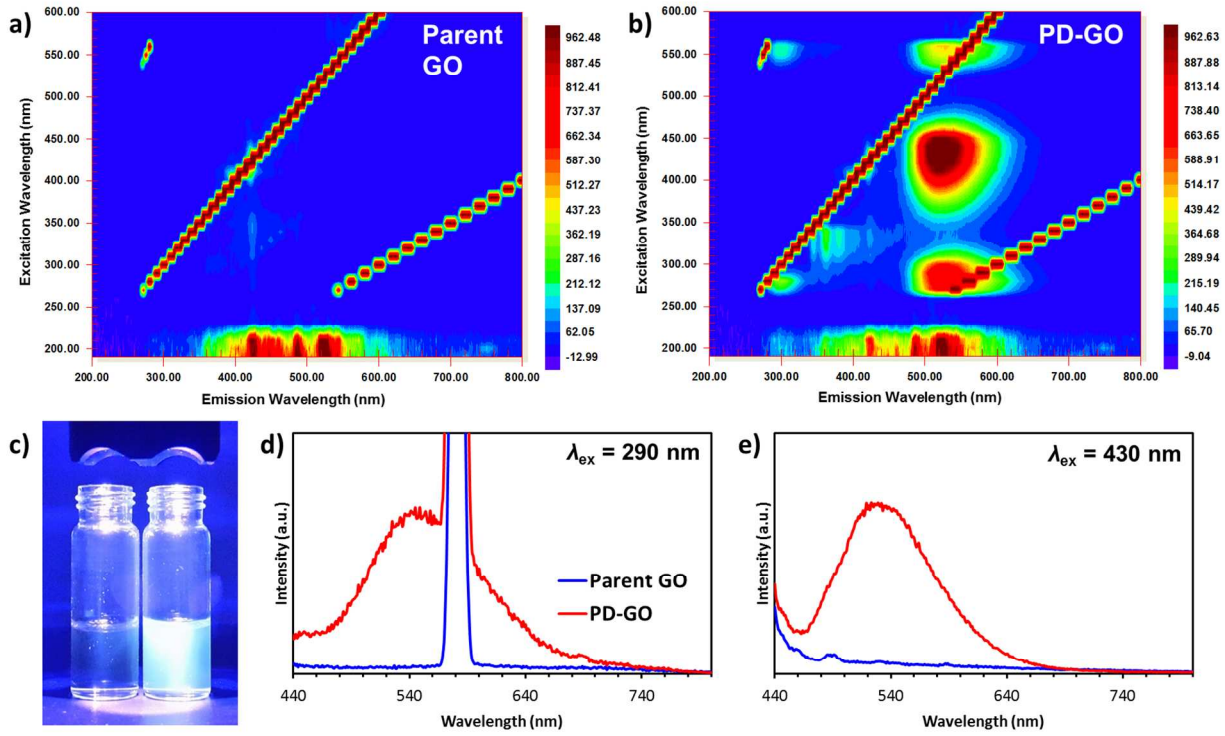

Figure 4. Fluorescence of parent GO and PD-GO in *N*,*N*-dimethylformamide at 0.1 mg mL^{-1}. Dependence of fluorescence on wavelength of the excitation light for **a)** parent GO, and **b)** PD-GO. High intensity lines are due to scattering of the excitation light and its second order. **c)** Dispersions of parent GO (left) and PD-GO (right) under illumination from a 365 nm UV light source. Emission spectra of parent GO and PD-GO at **(d)** 290 nm and **(e)** 430 nm excitation wavelengths.

We consequently investigated the origin for fluorescence in PD-GO, particularly the localisation of sp^2 domains which is a generally accepted mechanism for graphene fluorescence.[30,32-35,56,57] Gradient centrifugation of the GO dispersions was first performed (at increasing speeds of 1000, 3000, 6000, and 9000 rpm) to separate the sheets into their various sizes. Again, only PD-GO showed fluorescence and the smallest PD-GO sheets from the 9000 rpm supernatant exhibited strongest fluorescence intensities in the green visible region (Figure

S5 and S7). Their morphology appeared as few-layered stacks of highly fragmented sheets, with the smallest disk-shaped fragments down to approximately 50 nm in diameter (Figure 5f). The smallest parent GO sheets which did not exhibit any fluorescence are instead considerably larger of up to a few hundred nanometres across (Figure 5d). Both parent GO and PD-GO precipitates from 1000 rpm centrifugation (Figure 5c, 5d) were large multi-layered sheets a few micrometres wide. Additional structural information was also gleaned from Raman spectroscopy in Figure 5a-b, with the D (disorder) band at *ca*. 1350 cm^{-1} from an A_{1g} breathing mode arising from sp^3 defect sites while the G (graphitic) band occurs near 1560 cm^{-1} due to an E_{2g} mode from pristine sp^2 hybridised regions.[58] The ratio of the D to G bands (I_D/I_G ratio) in Figure 5g then provides an indication on the amount of sp^3 defects, with larger ratios signalling lesser pristine sp^2 structures. Thus, the average sp^2 crystallite sizes (L_a) can be derived from the equation:[59]

$$L_a = 2.4 \times 10^{-10} \times \lambda_{laser}^{4} \times I_G/I_D$$

where λ_{laser} is the wavelength of the excitation laser at 514.5 nm, and I_G and I_D are the integrated intensities of the Raman G and D bands. As tabulated in Figure 5h, average L_a sizes were found to decrease after PD labelling: from 8.6 to 7.1 nm for large sheets in the precipitate, but more significantly from 9.7 to 6.0 nm in the smallest supernatant sheets. As such, both the smallest sp^2 crystallite and physical sheet sizes observed in PD-GO fragments strongly suggest that sp^2 domain localisation and size confinement of the sheets occurred due to functionalisation, thus resulting in the observed fluorescence. The observation is in line with the labelling process forming new phenazine rings at the edge planes with *o*-quinones, and with oxygen functionalities which border pristine sp^2 regions; both processes would contribute to the overall decrease in the pristine sp^2 domain size throughout the basal plane.

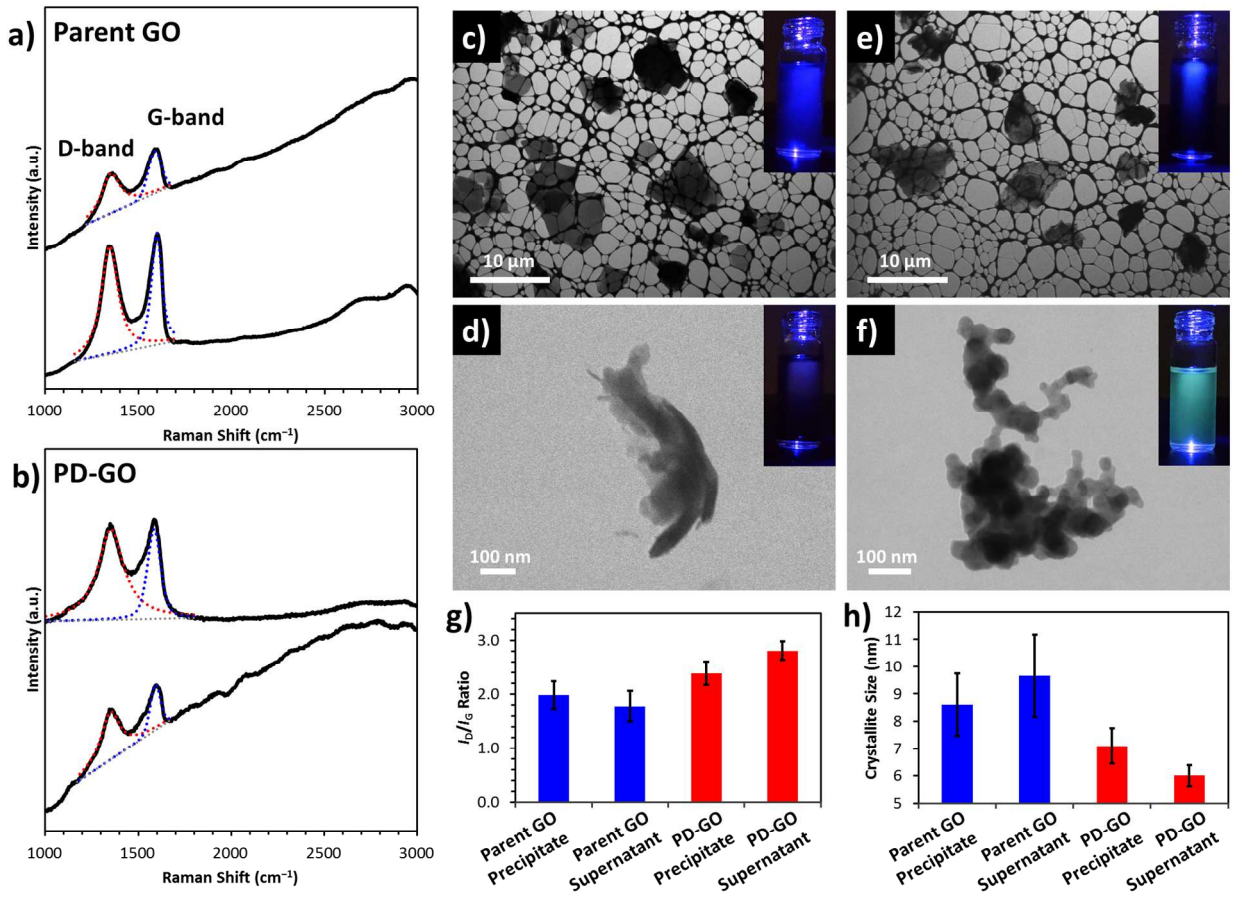

Figure 5. Raman spectra of the parent GO **(a)** and PD-GO **(b)**; top spectrum corresponds to the precipitate after centrifugation at 1000 rpm for 20 mins and the bottom spectra is obtained from the supernatant after centrifugation at 9000 rpm (λ_{exc}=514.5 nm). Scanning transmission electron images of the parent GO precipitate **(c)** and supernatant **(d)**, and PD-GO precipitate **(e)** and supernatant **(f)**; Inset figures show the particle dispersions under 365 nm UV light irradiation. Comparison of the D to G band intensity ratios from Raman spectra **(g)** and calculated sp^2 crystallite sizes **(h)**. Error bars represent the standard deviation, n = 5.

The effect of size and fraction of sp^2 regions on the bandgap has been previously established, where the bandgap of the graphene material decreases with increasing size of an sp^2 cluster tending towards an approximate 2.1 eV for clusters of ~37 rings.[34,56,57] For our case with PD-GO, the emission peak at ~540 nm corresponds to a bandgap of ~2.3 eV close to the calculation by Eda *et al*.[34] This is further supported by the similarity in fluorescence excitation and emission wavelengths from benzenediamine-functionalised graphene quantum dots at 410 nm and 502 nm

respectively, and the red shift for PD-GO in the present case can be fittingly attributed to the larger π-conjugation system as we have seen.[56] The main difference however is that PD-GO undergoes excitation over both the UV and visible ranges, at the optimal wavelengths of 290 nm and 430 nm (Figure 4d-e). Nonetheless if we consider that the phenazine moiety is itself a chromophore which also absorbs light at *ca*. 250 nm,[60,61] we may postulate that these groups serve as additional sites for light absorption which are once again red shifted due to conjugation. Consequently, the energy is transferred to the emission sites[30] on PD-GO resulting in fluorescence at 540 nm. Hence, based on the similar 540 nm emission wavelength regardless of UV and visible excitations, we may conclude that it is from the same localised sp^2 regions that the fluorescence of PD-GO originates.

3. Conclusions

We report the chemical labelling of graphene oxide (GO) with 1,2-phenylenediamine (PD) to produce a multifunctional GO material exhibiting superior capacitive charge storage ability in addition to enhanced fluorescence properties. While many capacitor devices are based on EDLCs, in this study however, an alternative approach to enhance GO pseudo-capacitance is used instead. The production of labelled PD-GO involves a fast and simple one-step GO functionalization that is cost-effective. A common problem of poor electrical conductivity in GO is also addressed. Effects such as surface area and pore-size were found to not have contributed to the large specific capacitance of PD-GO, but which arises from pseudo-capacitance of the phenazine groups after labelling. Interestingly, a yellow-green fluorescence was also observed, which we attribute to the effect of sp^2 domain localisation on the bandgap, and also UV absorbance of the phenazine adduct. The results suggest that future design of functionalized GO

materials may similarly lead to their application in various diverse fields such as electronics and optical devices.

4. Experimental Section

4.1. Materials

Graphite (<20 mm), sulfuric acid (95–98%), hydrochloric acid (37%), glacial acetic acid, hydrogen peroxide (30%), N,N-dimethylformamide (DMF), ethanol, diethyl ether, sodium nitrate, potassium phosphate dibasic, and sodium phosphate monobasic were purchased from Sigma–Aldrich (Singapore). 1,2-phenylenediamine (PD) was obtained from Alfa Aesar. Potassium permanganate and fuming nitric acid (>90%) were purchased from J.T. Baker. Glassy carbon (GC) electrodes (3 mm diameter) and a platinum auxiliary electrode were obtained from CH Instruments (USA). Milli-Q water (resistivity at 18.2 MΩ cm) was used throughout the study. Electrochemical measurements were performed in a 5 mL electrochemical cell using a three-electrode configuration connected to an Autolab PGSTAT 101 (Eco Chemie, Utrecht, The Netherlands).

4.2. GO preparation via the modified Hummers Method.[62]

0.5 g of graphite was first added to sulfuric acid (23.0 mL, 95–98%) at 0 ^{o}C and stirred for 20 min, followed by portion-wise addition of 0.5 g $NaNO_3$ with stirring for 1 h. $KMnO_4$ (3 g) was then added slowly with temperature kept at 0 ^{o}C, with subsequent heating to 35 ^{o}C for 1 h. 40 mL of water was then added to the mixture which resulted in the temperature rising to ~90 ^{o}C and maintained for 30 min. An additional 100 mL of water was added, followed by slow addition

of approximately 10 mL H_2O_2 (30%). The warm solution was filtered through a reconstituted cellulose membrane (0.22 μm) and washed with warm water (100 mL). Finally, the solid was washed copiously with water until a neutral pH was achieved and dried under vacuum at 50 ^oC for five days before use.

4.3. Labelling with 1,2-Phenylenediamine (PD)[37,38]

GO (20 mg) was first dispersed in glacial acetic acid at 1 mg mL^{-1} concentration for 1 h with ultrasonication. In a second flask, 1,2-phenylenediamine (77 mg) was dissolved in EtOH (2 mL) and then added to the GO suspension. For the control experiment, only pure EtOH was added. The mixture was then stirred for 1 h at 95 ^oC. The labelled GO was obtained by vacuum filtration and washed sequentially with EtOH, water, and ether, and the pH increasing to a final value of *ca*. 6. The labelled GO was lastly dried in a vacuum oven for 48 hours before usage.

4.4. Materials and Electrochemical Characterization

X-ray photoelectron spectroscopy was performed with a Phoibos 100 spectrometer using an Mg Kα source (SPECS, Germany). Relative sensitivity factors were used for calculation of elemental compositions and carbon-to-oxygen (C/O) ratios. Samples were compressed onto carbon tape mounted on aluminum holders. Raman spectroscopy was done on a confocal micro-Raman LabRam HR instrument (Horiba Scientific) in backscattering geometry with a CCD detector, using a 514.5 nm Argon excitation laser and a 100× objective mounted on an Olympus optical microscope giving a laser spot-size of approximately 5–10 μm. Calibration was achieved using a silicon reference with a peak position at 520 cm^{-1} and a resolution of less than 1 cm^{-1}. Scanning transmission electron microscopy was performed using a JEOL 7600F field-emission

scanning electron microscope (JEOL, Japan) operated at an accelerating voltage of 30 kV with concurrent measurement of energy dispersive X-ray spectra. Samples were deposited onto lacey carbon copper grids (Ted Pella, USA) using a 0.1 mg mL^{-1} dispersion in DMF. N_2 adsorption/desorption analysis was performed with a Quantachrome Instruments Nova 2200e BET surface area and pore size analyzer at 77.4 K. Sample de-gassing was performed at 110 ^oC for 20 h to prevent loss of inherent functionalities. Pore analyses were performed with the NovaWin software (Quantachrome Instruments, USA), with non-local density functional theory (NLDFT) calculations using an equilibrium slit-pore model on carbon. The method is an accepted standard for pore characterisation that allows for both micro- and meso-pore analysis, and the carbon slit pore model was chosen as it approximates the planar graphitic sheets in graphene-type materials. The reference isotherm and model parameters are described in Ravikovitch *et al*.[63]

Electrical conductivity measurements were performed on a gold interdigitated array electrode (ALS Corporation, Japan) by deposition of a 2.0 μL suspension of the relevant material (at 1 mg mL^{-1} concentration in deionised water) onto the interdigitated region 2 mm wide (individual gold contacts are spaced 10 μm apart) and dried in air. Linear sweep voltammetric scans were performed at a scan rate of 0.02 V s^{-1}. Fluorescence was investigated using a Cary Eclipse fluorescence spectrophotometer (Varian, USA) in quartz cuvettes with a 0.1 mg mL^{-1} suspension of the material in DMF. A high photomultiplier tube voltage was employed for the detector. GC electrode surfaces were renewed by polishing with a 0.05 μm alumina particle slurry on a polishing pad and washed subsequently with copious amounts of deionized water prior to measurement. All electrochemical potentials are relative to the Ag/AgCl reference electrode. For

studies on capacitor performance, cyclic voltammetry and galvanostatic charge/discharge measurements were performed in 6 M KOH. Capacitance values are only calculated from discharge cycles after they have stabilized past the initial few charge/discharge cycles. 1.0 μL aliquots of each GO at a 5.0 mg mL^{-1} concentration in DMF were used, giving a loading capacity of 70.7 μg cm^{-2} per electrode.

Corresponding Author

*Martin Pumera. Email: pumera@ntu.edu.sg

Acknowledgements

M.P. acknowledges a Tier 2 grant (MOE2013-T2-1-056; ARC 35/13) from the Ministry of Education, Singapore.

References

1. R. Raccichini, A. Varzi, S. Passerini and B. Scrosati, *Nat. Mater.*, 2015, **14**, 271–279.

2. Z. Yang, J. Ren, Z. Zhang, X. Chen, G. Guan, L. Qiu, Y. Zhang and H. Peng, *Chem. Rev.*, 2015, **115**, 5159−5223.

3. K. Chen, S. Song, F. Liu and D. Xue, *Chem. Soc. Rev.*, 2015, **44**, 6230−6257.

4. Y. Zhu, S. Murali, M. D. Stoller, K. J. Ganesh, W. Cai, P. J. Ferreira, A. Pirkle, R. M. Wallace, K. A. Cychosz, M. Thommes, D. Su, E. A. Stach and R. S. Ruoff, *Science*, 2011, **332**, 1537−1541.

5. Z. Yu, L. Tetard, L. Zhai and J. Thomas, *Energy Environ. Sci.*, 2015, **8**, 702−730.

6. H. Ji, X. Zhao, Z. Qiao, J. Jung, Y. Zhu, Y. Lu, L. L. Zhang, A. H. MacDonald and R. S. Ruoff, *Nat. Commun.*, 2014, **5**, 3317.

7. I. N. Kholmanov, C. W. Magnuson, R. Piner, J.-Y. Kim, A. E. Aliev, C. Tan, T. Y. Kim, A. A. Zakhidov, G. Sberveglieri, R. H. Baughman and R. S. Ruoff, *Adv. Mater.*, 2015, **27**, 3053–3059.

8. L. Cao, M. J. Meziani, S. Sahu and Y.-P. Sun, *Acc. Chem. Res.*, 2013, **46**, 171–180.

9. K. P. Loh, Q. Bao, G. Eda and M. Chhowalla, *Nat. Chem.*, 2010, **2**, 1015−1024.

10. I. A. Popov, K. V. Bozhenko and A. I. Boldyrev, *Nano Res.*, 2012, **5**, 117–123.

11. A. D. Zdetsis and E. N. Economou, *J. Phys. Chem. C*, 2015, **119**, 16991−17003.

12. J. Xia, F. Chen, J. Li and N. Tao, *Nat. Nanotech.*, 2009, **4**, 505–509.

13. J. Zhu, D. Yang, Z. Yin, Q. Yan and H. Zhang, *Small*, 2014, **10**, 3480–3498.

14. Z. Zuo, T. Y. Kim, I. Kholmanov, H. Li, H. Chou and Y. Li, *Small*, 2015, **11**, 4922–4930.

15. B. S. Mao, Z. Wen, Z. Bo, J. Chang, X. Huang and J. Chen, *ACS Appl. Mater. Interfaces*, 2014, **6**, 9881–9889.

16. J. Luo, H. D. Jang and J. Huang, *ACS Nano*, 2013, **7**, 1464–1471.

17. I.-Y. Jeon, Y.-R. Shin, G.-J. Sohn, H.-J. Choi, S.-Y. Bae, J. Mahmood, S.-M. Jung, J.-M. Seo, M.-J. Kim, D. W. Chang, L. Dai and J.-B. Baek, *Proc. Natl. Acad. Sci. USA*, 2012, **109**, 5588–5593.

18. R. Nandhini, P. A. Mini, B. Avinash, S. V. Nair and K. R. V. Subramanian, *Mater. Lett.*, 2012, **87**, 165–168.

19. A. J. Pak, E. Paek and G. S. Hwang, *J. Phys. Chem. C*, 2014, **118**, 21770–21777.

20. S. Kerisit, B. Schwenzer and M. Vijayakumar, *J. Phys. Chem. Lett.*, 2014, **5**, 2330–2334.

21. A. J. Pak, E. Paek and G. S. Hwang, *Carbon*, 2014, **68**, 734–741.

22. M. A. Pope and I. A. Aksay, *J. Phys. Chem. C*, 2015, **119**, 20369–20378.

23. A. Ambrosi, H. L. Poh, L. Wang, Z. Sofer and M. Pumera, *ChemSusChem*, 2014, **7**, 1102–1106.

24. M. A. Pope, C. Punckt and I. A. Aksay, *J. Phys. Chem. C*, 2011, **115**, 20326–20334.

25. N. A. Kumar, H.-J. Choi, Y. R. Shin, D. W. Chang, L. Dai and J.-B. Baek, *ACS Nano*, 2012, **6**, 1715–1723.

26. Y. Liu, R. Deng, Z. Wang and H. Liu, *J. Mater. Chem.*, 2012, **22**, 13619–13624.

27. H. Wang, Q. Hao, X. Yang, L. Lu and X. Wang, *Electrochem. Commun.*, 2009, **11**, 1158–1161.

28. J. Ji, Y. Li, W. Peng, G. Zhang, F. Zhang and X. Fan, *Adv. Mater.*, 2015, **27**, 5264–5279.

29. X. Cui, R. Lv, R. U. R. Sagar, C. Liu and Z. Zhang, *Electrochim. Acta*, 2015, **169**, 342–350.

30. H. R. Thomas, C. Vallés, R. J. Young, I. A. Kinloch, N. R. Wilson and J. P. Rourke, *J. Mater. Chem. C*, 2013, **1**, 338–342.

31. J. Shang, L. Ma, J. Li, W. Ai, T. Yu and G. G. Gurzadyan, *Sci Rep.*, 2012, **2**, 792.

32. C.-T. Chien, S.-S. Li, W.-J. Lai, Y.-C. Yeh, H.-A. Chen, I.-S. Chen, L.-C. Chen, K.-H. Chen, T. Nemoto, S. Isoda, M. Chen, T. Fujita, G. Eda, H. Yamaguchi, M. Chhowalla and C.-W. Chen, *Angew. Chem. Int. Ed.*, 2012, **51**, 6662–6666.

33. S. Zhu, S. Tang, J. Zhang and B. Yang, *Chem. Commun.*, 2012, **48**, 4527-4539.

34. G. Eda, Y.-Y. Lin, C. Mattevi, H. Yamaguchi, H.-A. Chen, I.-S. Chen, C.-W. Chen and M. Chhowalla, *Adv. Mater.*, 2010, **22**, 505–509.

35. Q. S. Mei, K. Zhang, G. Guan, S. Wang and Z. Zhang, *Chem. Commun.*, 2010, **46**, 7319–7321.

36. Y. Xu, Z. Liu, X. Zhang, Y. Wang, J. Tian, Y. Huang, Y. Ma, X. Zhang and Y. A. Chen, *Adv. Mater.*, 2009, **21**, 1275–1279.

37. C. A. Thorogood, G. G. Wildgoose, A. Crossley, R. M. J. Jacobs, J. H. Jones and R. G. Compton, *Chem. Mater.*, 2007, **19**, 4964–4974.

38. G. G. Wildgoose, P. Abiman and R. G. Compton, *J. Mater. Chem.*, 2009, **19**, 4875–4886.

39. T. Szabó, O. Berkesi, P. Forgó, K. Josepovits, Y. Sanakis, D. Petridis and I. Dékány, *Chem. Mater.*, 2006, **18**, 2740–2749.

40. W. Scholz and H. P. Boehm, *Z. Anorg. Allg, Chem.*, 1969, **369**, 327.

41. H. He, J. Klinowski, M. Forster and A. Lerf, *Chem. Phys. Lett.*, 1998, **287**, 53–56.

42. A. M. Dimiev, L. B. Alemany and J. M. Tour, *ACS Nano*, 2013, **7**, 576–588.

43. C. K. Chua, Z. Sofer and M. Pumera, *Chem.—Eur. J.*, 2012, **18**, 13453–13459.

44. D. R. Dreyer, S. Park, C. W. Bielawski and R. S. Ruoff, *Chem. Soc. Rev.*, 2010, **39**, 228–240.

45. A. Y. S. Eng, A. Ambrosi, C. K. Chua, F. Šaněk, Z. Sofer and M. Pumera, *Chem.—Eur. J.*, 2013, **19**, 12673–12683.

46. E. Bekyarova, M. E. Itkis, P. Ramesh, C. Berger, M. Sprinkle, W. A. de Heer and R. C. Haddon, *J. Am. Chem. Soc.*, 2009, **131**, 1336–1337.

47. Y. Feng, H. Liu, W. Luo, E. Liu, N. Zhao, K. Yoshino and W. Feng, *Sci. Rep.*, 2013, **3**, 3260.

48. A. Y. S. Eng, C. K. Chua and M. Pumera, *Nanoscale*, 2015, **7**, 20256–20266.

49. C. K. Chua and M. Pumera, *Chem.—Eur. J.*, 2013, **19**, 2005–2011.

50. L. Buglione, E. L. K. Chng, A. Ambrosi, Z. Sofer and M. Pumera, *Electrochem. Commun.*, 2012, **14**, 5–8.

51. B. Xu, S. Yue, Z. Sui, X. Zhang, S. Hou, G. Cao and Y. Yang, *Energy Environ. Sci.*, 2011, **4**, 2826–2830.

52. P. Simon, Y. Gogotsi and B. Dunn, *Science*, 2014, **343**, 1210–1211.

53. J. E. Zuliani, J. N. Caguiat, D. W. Kirk and C. Q. Jia, *J. Power Sources*, 2015, **290**, 136–143.

54. P. Simon and Y. Gogotsi, *Acc. Chem. Res.*, 2013, **46**, 1094–1103.

55. C. Largeot, C. Protet, J. Chmiola, P.-L. Taberna, Y. Gogotsi and P. Simon, *J. Am. Chem. Soc.*, 2008, **130**, 2730–2731.

56. B.-P. Qi, H. Hu, L. Bao, Z.-L. Zhang, B. Tang, Y. Peng, B.-S. Wang and D.-W. Pang, *Nanoscale*, 2015, **7**, 5969–5973.

57. S. Vempati and T. Uyar, *Phys. Chem. Chem. Phys.*, 2014, **16**, 21183–22103.

58. A. C. Ferrari and D. M. Basko, *Nat. Nanotechnol.*, 2013, **8**, 235–246.

59. L. G. Cançado, K. Takai, T. Enoki, M. Endo, Y. A. Kim, H. Mizusaki, A. Jorio, L. N. Coelho, R. Magalhães-Paniago and M. A. Pimenta, *Appl. Phys. Lett.*, 2006, **88**, 163106.

60. G. A. Swan and D. G. I. Felton, in *Chemistry of Heterocyclic Compounds: Phenazines*, *Vol. 11*, John Wiley & Sons, Hoboken, NJ, USA, 1957, pp-14-27.

61. W. Huang, L. Sun, Z. Zheng, J. Su and H. Tian, *Chem. Commun.*, 2015, **51**, 4462.

62. W. S. Hummers and R. E. Offeman, *J. Am. Chem. Soc.*, 1958, **80**, 1339–1339.

63. P. I. Ravikovitch, A. Vishnyakov, R. Russo and A. V. Neimark. *Langmuir*, 2000, **16**, 2311-2320.

Table of Contents Entry

Labelling of graphene oxide with *o*-phenylenediamine produces an interesting nanomaterial exhibiting dual enhancements in its capacitance and fluorescence properties.